JOURNAL OF ENZYME INHIBITION AND MEDICINAL CHEMISTRY
2025, VOL. 40, NO. 1, 2482892
https://doi.org/10.1080/14756366.2025.2482892

Taylor & Francis
Taylor & Francis Group

RESEARCH ARTICLE

OPEN ACCESS Check for updates

Tetra-anionic porphyrin mimics protein-protein interactions between regulatory particles and the catalytic core, allosterically activating human 20S proteasome

A. M. Santoro[a*], M. Persico[b*], A. D'Urso[c], A. Cunsolo[c,d], O. Tkachuk[b], D. Milardi[a], R. Purrello[c], G. R. Tundo[e], D. Sbardella[f], P. A. Osmulski[g], M. Gaczynska[g], M. Coletta[f] and C. Fattorusso[b]

[a]National Research Council, Institute of Crystallography, Sede Secondaria di Catania, Catania, Italy; [b]Department of Pharmacy, University of Naples "Federico II", Napoli, Italy; [c]Department of Chemical Sciences, University of Catania, Catania, Italy; [d]Epic Sciences, San Diego, California, USA; [e]Department of Clinical Sciences and Translational Medicine, University of Roma Tor Vergata, Roma, Italy; [f]IRCCS-Fondazione BIETTI, Rome, Italy; [g]Department of Molecular Medicine, University of Texas Health at San Antonio, San Antonio, Texas, USA

ABSTRACT

Decreased proteasome activity is a hallmark of brain and retinal neurodegenerative diseases (Alzheimer's, Parkinson's diseases, glaucoma) boosting the search for molecules acting as proteasome activators. Based on the hypothesis of an electrostatic key code driving catalytic core particle (20S) activation by regulatory particles (RPs), we identified the tetra-anionic meso-Tetrakis(4-sulphonatophenyl)-porphyrin (H2TPPS) as a new activator of human proteasome. By means of an integrated approach, including bioinformatics, enzymatic kinetic analysis, atomic force microscopy, and dynamic docking simulations, we show how binding of H2TPPS affects the closed/open conformational equilibrium of human 20S to ultimately promote substrate gate opening and proteolytic activity. These outcomes support our hypothesis and pave the way to the rational discovery of new proteasome allosteric modulators able to reproduce the key structural elements of regulatory particles responsible for catalytic activation.

ARTICLE HISTORY
Received 9 October 2024
Revised 3 March 2025
Accepted 11 March 2025

KEYWORDS
Proteasome; activator; allostery; electrostatic code; h20S conformational states

Introduction

Proteasome is a predominantly cytosolic multi-subunit protease that constitutes the focal point of the ubiquitin-proteasome pathway (UPP), the major venue of regulated protein catabolism[1–4]. Proteasome is broadly involved in the regulation of many key metabolic processes and its malfunction is directly linked to the pathogenesis of a large number of diseases, spanning from cancer to brain and retinal/optic nerve neurodegeneration[1,5–7].

The mature proteasome is composed of a barrel-shaped core particle (20S CP; human 20S proteasome (h20S)), which harbours the catalytic subunits, and different regulatory particles (RPs; namely 19S, PA28, and PA200 in the case of h20S) that may bind to the core[8–10]. There is also a number of other modulators (e.g. Ecm29[11], heat shock protein 60 (HSP60)[12] insulin-degrading enzyme (IDE)[13] Catalytic Core Regulators (CCRs)[14]) often referred to as proteasome interacting proteins (PIPs)[15,16]. The 20S CP is made by four heptameric stacked rings, namely two external α rings (α1–α7) and two inner β rings (β1-β7)[17,18]. Each β-heptamer contains the catalytic subunits β1, β2, and β5, which exhibit postglutamyl peptide hydrolysing (PGPH), trypsin-like (T-L), and chymotrypsin-like (ChT-L) cleavage activity, respectively[19]. Substrate access to the catalytic chambers occurs through the gate placed in the centre of the surface of each of the two α-rings. In the absence of a substrate and/or activators (e.g. RPs) the gate is mostly closed, and the closure is guaranteed by the N-terminal tails of α2, α3, and α4 subunits, which occupy the top of the central substrate channel. Proteasome activation, also assisted by RPs, is regulated through complex conformational equilibria involving a dynamic cross-talk between α and β subunits, resulting in a tight control of α rings and the gate to finely tune the substrate's access to catalytic sites inside the 20S CP barrel[20–25].

Due to its broad involvement in the cell's physiology the proteasome emerged as an attractive pharmacological target[7,26]. Anti-cancer actions of specific competitive proteasome inhibitors are best known, with several drugs used in clinics. Apart from inhibition of hyperactive proteasomes in cancerous cells, boosting the activity of proteasomes in neurodegenerative disorders[27,28] and retinal disease[29], both associated to UPP decline, is worth recognition. In this scenario, proteasome activation turned out to be effective to reduce proteotoxicity *in cells*[30–33] and also to attenuate symptoms of neurodegeneration in animal models of Alzheimer's disease[34]. In addition, increased proteasome activity has been observed in the exceptionally long-lived naked male rat[35,36] and long-lived humans (centenarians)[37], consistent with the notion that progressive decline in UPP effectiveness contributes to deleterious effects of senescence[38]. Based on these evidences, strategies have been developed to increase UPP activity in the fight against

CONTACT M. Coletta massimiliano.coletta@fondazionebietti.it IRCCS-Fondazione BIETTI, Rome, Italy; C. Fattorusso caterina.fattorusso@unina.it Department of Pharmacy, University of Naples "Federico II", Via D. Montesano 49, Napoli 80131, Italy
*These authors equally contributed.

Supplemental data for this article can be accessed online at https://doi.org/10.1080/14756366.2025.2482892.

neurodegenerative and eye diseases, with several compounds identified as potential proteasome activators[32]. These activators can be classified into (*i*) direct or (*ii*) indirect; the former consists of molecules that bind directly to the 20S proteasome and enhance its proteolytic activity, while the latter includes compounds able to boost the proteasome actions through the regulation of its transcription factors, deubiquitinases, and upstream kinases[39–41].

Direct proteasome activators are often reported to act as gate openers and are represented by either synthetic or natural compounds that, by relaxing the narrow 20S gate, promote substrate entry into the catalytic chamber of the 20S core. Several peptides of distinct origins have been identified as direct activators/gate openers. Some of them are derived from RPs, most notably the conserved HbYX (Hb = hydrophobic; Y = Tyr; X = any residue) activating motif present at the 20S-binding C-terminals of PA200 and the 19S Rpt (regulatory particle ATPase) subunits 2, 3, and 5[42–46]. Specifically designed peptide-based compounds include the HbYX-like dipeptide mimetic Z-Tyr-Ala (ZYA)[30] chimeric peptides of Cathelicidins with the RP C-terminal HbYX motif[47], Trans-Activator of Transcription (TAT)-derived peptides[48].

Multiple small-molecule ligands have been reported as direct proteasome activators as well, among them several natural compounds, such as ursolic, betulinic, oleanolic acids[49], lithocholic acid[50], cycloastragenol[51], polyphenols[52,53], aflatoxins[54], sylibins[55], oleuropein[56], citicoline[57], and syrosingopine[58]. On the other hand, direct proteasome activators have also been found among synthetic small molecules from varied structural classes, including fluspirilene analogs, phenotiazines, dihydroquinazolines[59], pyrazolones[60], imidazolines[61], MK886 and its derivatives[62], N-arachidonoylphenolamine (AM404)[63], carboranes[64], and a cytisine derivative[65].

Recently, we have identified cationic porphyrins as a new class of proteasome modulators[66–69] which, according to our hypothesis, are able to interact with charged residues located in the grooves between the α subunits. Importantly, such residues are also involved in ionic interactions with RPs. We postulate that these interactions may represent the "electrostatic key code" able to fine-tune the ability of charged ligands to interfere with the proteasome gate movements. Porphyrins, with their constrained and perfectly symmetric planar structure, represent valuable chemical probes for assessing the validity of our hypothesis. The chemical amenability to facile modification of the porphyrins' side groups enables structure-activity relationships (SARs) studies. This translates into a rational design of modifications of the porphyrin scaffold in order to generate compounds that exert desired effects on the proteasome enzymatic capabilities.

In line with our "electrostatic key code" hypothesis, we recently reported[69] the diverse effects of changing the number of charged groups and, at the same time, introducing a hydrophobic moiety in the porphyrin structure by the replacement of one of the protonated N-methyl pyridine substituents of meso-tetrakis(4-N-methylpyridyl)-porphyrin (H2T4) with a phenyl ring (Figure 1).

The resulting compound, 5-(phenyl)-10,15,20-(tri N-methyl-4-pyridyl)-porphyrin (TrisT4), displayed an activating effect on h20S and this was ascribed to the ability of the introduced phenyl ring to mimic a key interaction of the HbYX activating motif at the C-terminals of 19S and PA200[69]. However, the increase of substrate concentration resulted in diminishing the enzymatic activity. Namely, the activating effect of TrisT4 was no longer detectable at substrate concentration >25μM. Enhancing the ChT-L activity of h20S was also observed with 5,10,15-Tri(N-methyl-4-piridyl) corrole (TMPC; Figure 1), however the activation was followed by inhibition upon increasing ligand concentration[67].

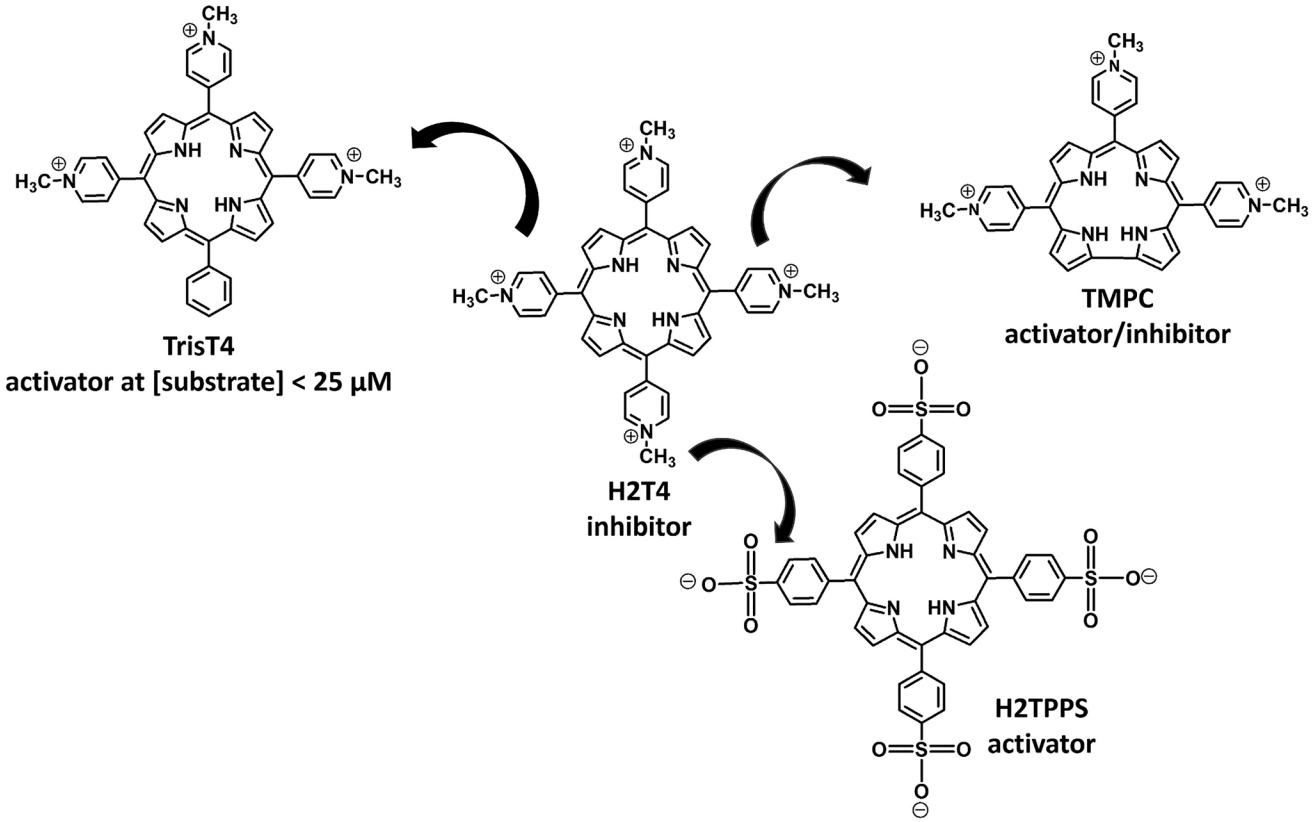

Figure 1. 2D structures of cationic and anionic porphyrins identified as 20S inhibitors or activators.

Based on the map of the ionic interactions between charged residues present on the surface of h20S α-ring and the docking regions of RPs[66], herein, we have extended our SAR study and investigated the effect of changing the electrostatic charges on the porphyrin scaffold from positive to negative. Accordingly, we report the effect of a tetra-anionic porphyrin derivative, meso-tetrakis (4-sulphonatophenyl)-porphyrin (H2TPPS; Figure 1) on the ChT-L activity of h20S. Moreover, we have used single-molecule imaging by atomic force microscopy (AFM) to monitor the conformational equilibria of the h20S gate area (closed, intermediate, and open state) upon exposure to this porphyrin, and we performed dynamic docking simulations to investigate the binding of H2TPPS to the different h20S conformations.

Overall, our findings on the capacity of charged porphyrins to interact with the electrostatic array present on the surface of the 20S α-rings indicate a specific influence of anionic groups in regulating the proteasome gating mechanisms, thereby validating our "electrostatic key code" hypothesis.

Materials and methods

Chemicals

Purified human 20S proteasome was purchased either from Bio-Techne (Minneapolis, Minnesota, USA), or from Enzo Life Sciences, Inc. (Farmingdale, NY, USA). The fluorogenic substrates specific for the chymotryptic-like (ChT-L) proteasome activity (succinyl-LeuLeuValTyr-7-amido-4-methylcoumarin; Suc-LLVY-AMC) was purchased from Bio-Techne (Minneapolis, Minnesota, USA).

H2TPPS (Figure 1) was purchased from Mid-century Chemicals (Chicago, IL). Porphyrin stock solutions were prepared by dissolving a small amount of H2TPPS solid in ultrapure water obtained from Elga Purelab Flex system by Veolia (Aubervilliers, France). The concentration was calculated in the UV region using the extinction coefficient of 4.8×10^5 $M^{-1}cm^{-1}$ at λ = 412 nm. To avoid protonation and aggregation of H2TPPS (pK_a = 5.8) the stock solutions were kept at pH 8 (with NaOH) at a concentration range between 1×10^{-4} M and 3×10^{-4} M.

Proteasome activity assays

Assays were performed in a 384 multiwells black flat bottom plate, in a final volume of 50 µl. The purified h20S proteasome (2 nM) was incubated for 30 min at 37 °C in the assay buffer Tris/HCl 50 mM at pH 8.0 with increasing concentrations (0.1–10 µM) of H2TPPS. Fluorogenic substrate Suc-LLVY-AMC, specific for ChT-L activity, was then added at concentrations from 5 to 100 µM. The enzymatic activity was assayed by continuously monitoring the fluorescence of the released 7-amino-4-methylcoumarin (AMC) for 30 min at 360/440 nm. A minimum of three replicates were performed for each data point. Data were analysed according to the following double-reciprocal Lineweaver–Burk equation,

$$\frac{[E_0]}{v} = \frac{K_m}{k_{cat}} \times \frac{1}{[S]} + \frac{1}{k_{cat}} \quad (1)$$

where $[E_0]$ is the enzyme concentration, v is the observed velocity (expressed as moles of substrate cleaved per time interval unit), and [S] is the substrate concentration. The resulting catalytic parameters were calculated, i.e. K_m (corresponding to the apparent affinity constant (or Michaelis–Menten constant) of substrate for the free enzyme (to form the ES complex)), and k_{cat} (corresponding to the velocity of the rate-limiting step during the enzymatic activity).

The physical interpretation of kinetic parameters can be referred to a mechanism, which may account for such a behaviour, represented by an allosteric ligand-linked model for *n* binding sites of H2TPPS to the 20S CP, wherefore the dependence of catalytic parameters, described by continuous lines in Figures 3A–C, has been carried out employing Equations (2a–c):

$$^{obs}k_{cat} = \frac{k_{catA}\cdot(1+\sigma_A\cdot K_{AL}\cdot[H2TPPS])^n + L_L\cdot k_{catB}\cdot(1+\sigma_B\cdot K_{BL}\cdot[H2TPPS])^n}{(1+K_{AL}\cdot[H2TPPS])^n + L_L\cdot(1+K_{BL}\cdot[H2TPPS])^n} \quad (2a)$$

$$^{obs}K_m = {}^{0}K_m\cdot\frac{(1+K_{AU}\cdot[H2TPPS])^n + L_U\cdot(1+K_{BU}\cdot[H2TPPS])^n}{(1+K_{AL}\cdot[H2TPPS])^n + L_L\cdot(1+K_{BL}\cdot[H2TPPS])^n} \quad (2b)$$

$$\frac{^{obs}k_{cat}}{^{obs}K_m} = \frac{k_{catA}\cdot\left(1+\sigma_A\cdot K_{AL}\cdot[H2TPPS]\right)^n + L_L\cdot k_{catB}\cdot\left(1+\sigma_B\cdot K_{BL}\cdot[H2TPPS]\right)^n}{K_{mA}\left(\left(1+K_{AU}\cdot[H2TPPS]\right)^n + L_U\cdot\left(1+K_{BU}\cdot[H2TPPS]\right)^n\right)} \quad (2c)$$

where $^{obs}k_{cat}$, $^{obs}K_m$, $^{obs}k_{cat}/^{obs}K_m$ are the observed catalytic parameter at a given concentration of H2TPPS, $^{0}K_m$ corresponds to K_m in the absence of H2TPPS, *n* is the number of concerted allosteric binding sites for H2TPPS to 20S; k_{catA} and k_{catB} are the rates of the rate-limiting step of the two states A and B, respectively, σ_A and σ_B are interaction parameters, describing the effect on k_{cat} of H2TPPS binding to the A and B states, respectively. Additionally, K_{mA} and K_{mB} are the Michaelis-Menten constants for A and B states, K_{AU} and K_{BU} are the affinity constant for H2TPPS to 20S proteasome in the absence of substrate for the two states A and B, K_{AL} and K_{BL} are the affinity constant for H2TPPS to 20S proteasome in the substrate-bound ES complex. L_U is the equilibrium constant between the A and B states in the absence of the substrate, whereas L_L is the equilibrium constant between A and B in the substrate-bound ES complex. Interaction parameters α, β, γ and δ refer to the ratio between the affinity constant in the substrate-bound ES complex and in the absence of substrate, namely K_{AU}/K_{AL} (α), K_{BU}/K_{BL} (β), K_{BU}/K_{AU} (γ) and K_{BL}/K_{AL} (δ). In the case of human 20S, $n=2$ turned out to be the minimum value to account for the quite steep dependence of catalytic parameters, as reported in Figures 3A–C. Consequently, the overall mechanism can be described as in Scheme 1.

AFM imaging

Native, unfixed 20S proteasome particles were imaged with tapping (oscillating) AFM mode in liquid using our established procedure[48,70]. Briefly, purified human proteasomes (Enzo Life Sciences Inc.; Farmingdale, NY) in "imaging buffer" (5 mM Tris–HCl, pH 7) were deposited on freshly cleaved muscovite mica (Ted Pella Inc.; Redding, CA), which allowed for electrostatic immobilisation of the particles, majority of them in "top view" ("upright") position, attached to mica by their alpha ring surface and with the opposite-side alpha ring ("alpha face") conveniently exposed for analysis. The proteasomes, covered with the imaging buffer, were scanned and imaged with Sharp Nitride Lever (SNL) AFM probes with cantilevers of 0.35 N/m spring constants, with a scanner E of the Multimode Nanoscope IIIa (probes and instrument: Bruker Inc., Santa Barbara, CA). Gentle imaging in the height mode was achieved by using the amplitude setpoint between 1.4 and 1.8 V,

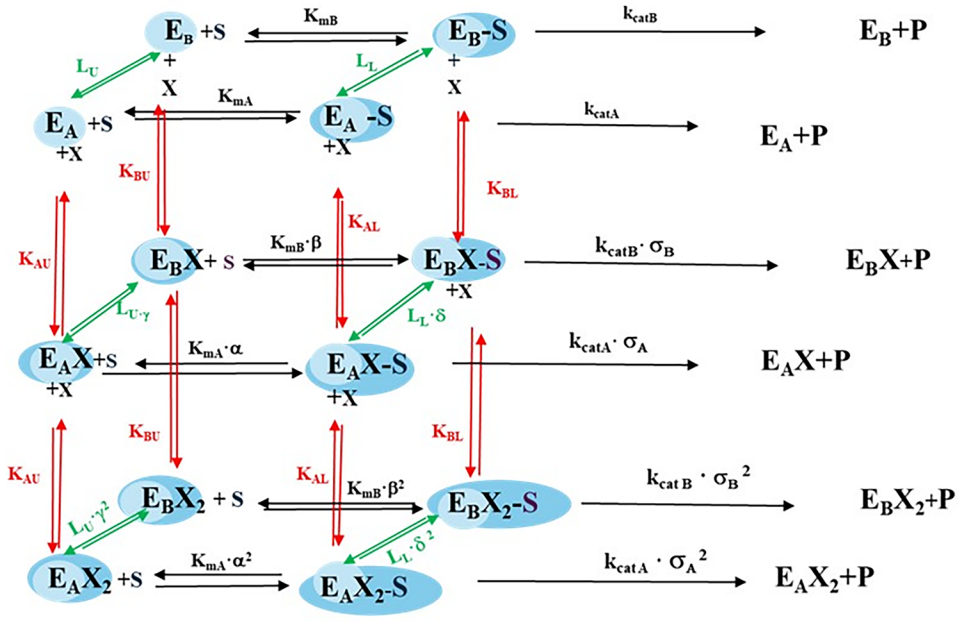

Scheme 1. Thermodynamic description of equilibria involved in the modulation of enzymatic activity of 20S proteasome (E) on the substrate (S) by the anionic porphyrin H2TPPS (X). Arrows indicate: equilibrium constants (green), kinetic parameters (black), ligand affinity constants (red). In the upper part is the scheme for the first H2TPPS binding step, while in the lower part is the scheme for the second H2TPPS binding step. Parameters concerning the enzymatic activity are depicted in black, those regarding porphyrin binding are depicted in red and conformational equilibria are depicted in green. (For the meaning of various parameters see text).

drive voltage of 200–500 mV, and scanning rate of 2.63 or 3.05 Hz (roughly 3 min per scan). Images of hundreds of 20S particles in multiple scanned 1 µm × 1 µm fields, trace and retrace, were collected with a digital resolution of 512×512 pixels. Selected fields were repeatedly scanned several times to monitor changes in topography of the same particles. Conformational response of proteasomes to the H2TPPS was followed by imaging the "control" particles first, and then injecting 10 µl of H2TPPS dissolved in imaging buffer directly into the AFM quartz wet imaging chamber. The proteasomes (6 nM) were exposed to 1 µM or 2 µM of the porphyrin (the final concentration). To test the response of control or H2TPPS – treated proteasomes to the model peptide substrate for ChT-L proteasome activity, the solution of Suc-LLVY–AMC was injected to the chamber to the final concentration of 100 µM, and the scanning continued. The topography of proteasomes was not affected by the injection process and by the presence of 1% DMSO (solvent for the Suc-LLVY-AMC), as was demonstrated previously[70].

The presented images of top-view 20S proteasomes are raw, since the only image processing applied was a standard 1st order plane-fit and flattening [NanoScope software version 5.12; Scanning Probe Image Processor (SPIP) version 6.0.13; Image Metrology, Hørsholm, Denmark] and brightness/contrast adjustments. The above softwares were also used for analysis of the dimensions of particles and the topography of the α face. Classification of the conformation of α face of a single top-view particle was carried outby analysing numerical values of the height of pixels in scan-lines crossing the area of the gate in the centre of the α face, as previously described[47,48,71]. Three conformational states of the α face and the gate were distinguished: closed (the plot of height values in the scan-line presented a convex function), intermediate (a concave function without a local minimum), and open (a central dip or, in other words, a local minimum detected). The data presented are averages of percent partition of the three conformers for the images of particles collected from at least three fields in at least two independent experiments (n = number of fields). 30–100 particles per field were routinely analysed. Significance of the differences between partitions for control ("idle") proteasomes and substrate or porphyrin treated 20S was determined with Chi-Square test (OriginPro 2020; OriginLab Corporation, Northampton, MA, USA).

Molecular modeling studies

Calculations were performed on CPU/GPU hybrid High Performance Computing Cluster (10 Twin servers, for a total of 560 Intel® Xeon® Gold processors (128 GB RAM), 64 AMD® EPYC® processors, and 2 GPU NVIDIA® Tesla® V100) and on E4 Server Twin 2×Dual Xeon 5520, equipped with two nodes. Each node: 2×Intel Xeon QuadCore E5520, 2,26Ghz, 36 GB RAM. The molecular modelling graphics were carried out on personal computer equipped with Intel(R) Core (TM) i7-8700 processor and SGI Octane 2 workstations.

A detailed description of the molecular modelling procedure is reported in the Supporting Information.

Results

Effect of H2TPPS on the h20S proteolytic activity

Figure 2 reports the double-reciprocal Lineweaver-Burk plot of data on the ChT-L enzymatic activity of h20S as a function of the fluorogenic substrate Suc-LLVY-AMC, specific for ChT-L activity, in the presence and in the absence of different H2TPPS concentrations, spanning from 0 to 10 µM.

It is immediately evident that the tetra-anionic porphyrin H2TPPS activates the h20S, at least over the investigated concentration range, bringing about an increase of the catalytic efficiency, as it comes from the decrease of the slope in the plot. However, this overall effect can be dissected into various contributions, namely the H2TPPS-linked effect on the velocity of the catalysis rate-limiting step (i.e. k_{cat}, see Figure 3A) and on the substrate affinity (i.e. K_m, see Figure 3B). The ratio between these two

contributions (i.e. k_{cat}/K_m, see Figure 3C) represents the actual catalytic efficiency of the enzyme.

The dependence of catalytic parameters on the H2TPPS concentration turns out to be cooperative, underlying an allosteric mechanism of this anionic porphyrin, whose binding induces a shift of the 20S proteasome from a functional state with a lower substrate affinity (which we call A state) towards one characterised by a higher substrate affinity (which we call B state).

Tables 1 and 2 report the parameters, as obtained by the application of Equations (1) and (2a-c) to experimental data, required to fully describe the H2TPPS-linked dependence of catalytic parameters for h20S, as reported in Figure 3.

Interestingly, as it comes from Table 1 in the absence of H2TPPS, h20S in the A state shows a slightly higher catalytic efficiency ($kcat/K_m$) than in the B state (6052 $M^{-1}s^{-1}$ vs 2133 $M^{-1}s^{-1}$). However, since H2TPPS has much higher affinity for the B compared to the A state (Table 2), then, the E_B–X_2 and E_B–X_2–S states are predominant by large in the (doubly liganded) fully activated h20S (as from $L_U \times \gamma^2 = 1.7 \times 10^4$ and $L_L \times \delta^2 = 1.4 \times 10^4$; see Scheme 1). By consequence, the corresponding enzymatic efficiency is defined by $k_{catB} \times \sigma_B^2/(K_{mB} \times \beta^2) = 1.6 \times 10^4$ $M^{-1}s^{-1}$, and resulted, in any case, increased with respect to that of the "initial" A or B states in the absence of H2TPPS (Figure 3C).

In summary, from a closer look at the whole of the data, it comes out that: (*i*) H2TPPS induces an activation of h20S through the concerted interaction of (at least) 2 molecules, bringing about a shift from the E_A to the E_BX_2–S conformational/functional state, (*ii*) the affinity of H2TPPS is very high for the B state, that is 75,000-fold higher than A in free enzyme and 19,000-fold higher than A in substrate-bound enzyme, (*iii*) such affinity is much higher than those of other porphyrins[67,69], envisaging the possibility that the site is positively charged, or, at least, it has a much higher affinity for negatively charged effectors.

AFM imaging

We used the AFM imaging to investigate the putative conformational changes induced in the proteasome gate area by H2TPPS binding. As in our previous studies, we found that the images of α face with the gate area of all core proteasome particles can be classified as "closed-gate", "intermediate" or "open-gate", depending on their topography[47,71] (Figure 4). As before[47,71], we found that all particles can freely assume any of the conformations when scanned and imaged repeatedly every 2–3 min. However, the

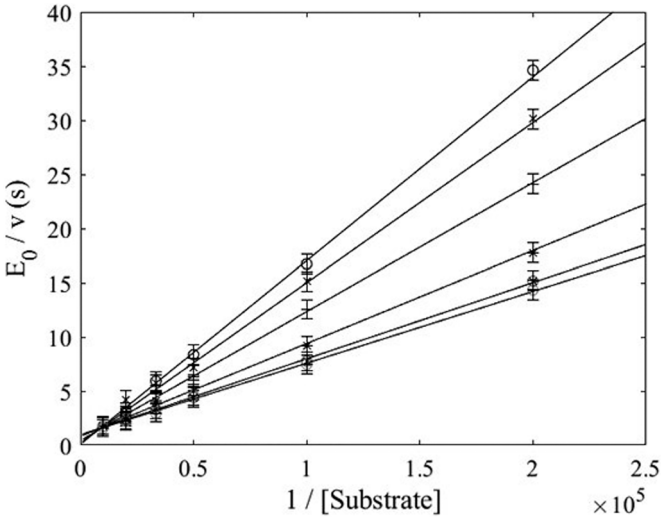

Figure 2. Lineweaver-Burk plot of the ChT-L activity of human 20S at pH 8.0 and 37 °C for different concentrations of H2TPPS porphyrin, namely no (o), 0.1 μM (x), 0.2 μM (+), 0.5 μM (*), 1 μM (⊗) and 10 μM (⊕). For the sake of simplicity data at 0.05 μM and at 5 μM H2TPPS have been omitted, since they were closely similar to those with no and 10 μM H2TPPS, respectively. Continuous lines are linear least-squares fitting of data according to Equation (1).

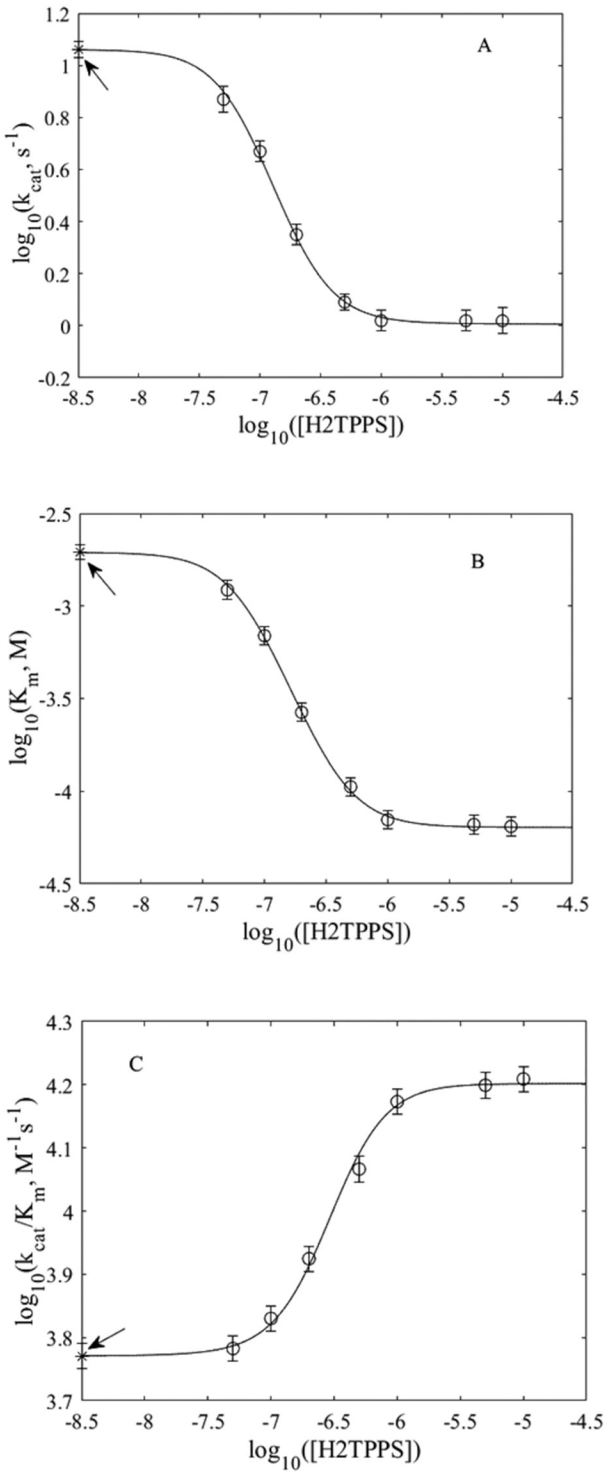

Figure 3. Dependence on H2TPPS concentration of ChT-L catalytic parameters of 20S proteasome, namely of kcat (panel A), Km (panel B) and kcat/Km (panel C). Continuous lines represent the non-linear least-squares fitting of data according to Equations (2a-c), employing the common set of parameters reported in Table 1. Asterisk, pointed by an arrow, indicates the parameter value in the absence of H2TPPS.

partition of conformers depended on the presence of specific ligands. Figure 4 demonstrates partitions of closed, intermediate, and open h20S particles in the absence or presence of the peptide substrate for the ChT-L activity and/or H2TPPS at two different concentrations (1 µM and 2 µM). The selected concentrations were within the range of functional effects on the ChT-L proteasome peptidase, as presented in Figures 2 and 3.

Consistently with our previous reports, control "idle" proteasomes in the absence of a substrate or a small molecule regulator existed in a conformational equilibrium of predominantly closed - gate forms (71% ± 3%), with a small representation of intermediate (22% ± 3%) and open – gate (7% ± 2%) particles (Figure 4, left). Upon addition of the peptide substrate, contribution of the closed conformers was reduced to only 21% ± 3%, with a significant increase of the contribution of intermediate (44% ± 4%) and open - gate conformers (35% ± 3%). Such partition was evident shortly after addition of the substrate, during the first scan (about 3 min), and remained stable through repeated scans. Addition of H2TPPS in the absence of a substrate induced a concentration-dependent reduction in closed-gate conformers; however, the reduction was relatively slow, with the partition of conformers stabilising after at least 15 min (5 scans) from the addition of the porphyrin (Figure 4, centre and right, compare "early" and "late" effects). Interestingly, treatment with 2 µM porphyrin resulted in the "late" partition of conformers not significantly different from that with the substrate alone (Figure 4, compare left and right). In turn, addition of the substrate to proteasomes treated with H2TPPS did not alter the conformers' make-up when 2 µM porphyrin was used and shifted the partition to "substrate-alone"—like when 1 µM porphyrin was used (Figure 4).

Table 1. Kinetic parameters of human 20S[69].

	h20S
k_{catA} (s^{-1})	11.5 ± 1.3
k_{catB} (s^{-1})	0.32 ± 0.05
K_{mA} (M)	1.9 (±0.4) × 10^{-3}
K_{mB} (M)	1.5 (±0.3) × 10^{-4}
L_U	3.0 (±0.5) × 10^{-6}
L_L	3.9 (±0.6) × 10^{-5}

Dynamic docking studies

Dynamic docking studies represent a valuable tool to model the interaction between enzymes and small molecules[72], in order to investigate the molecular bases of the ability of H2TPPS to affect the h20S conformational equilibrium, we docked the tetra-anionic ligand to the different conformational states of h20S (closed, "intermediate", and open). The aim was to explore possible binding sites for our tetra-anionic ligand and to identify the one characterised by the best binding energy. It is worth to underline that we docked one ligand molecule for each h20S conformational form, accordingly, no information was provided about the binding of additional ligand molecules to the same h20S conformer.

Ligand analysis and generation of the starting complexes

As a first step, the molecular model of H2TPPS was built (ionization state: tetra-anionic) and its conformational space was sampled. This allowed the identification of H2TPPS global minimum energy conformer and the subsequent calculation of ligand conformational energy in the docked complexes as well as the building of a pharmacophore model necessary for the generation of the binding hypothesis (Figure 5). Indeed, although during docking calculations the ligand is rotated and translated with respect to the protein and its conformation changed, nevertheless, the docking procedure formally requires a reasonable starting complex.

Table 2. Association constants of H2TPPS for the A and B states, unbound to substrate (K_{AU} and K_{BU}) and substrate-bound (K_{AL} and K_{BL}), number of H2TPPS molecules for full h20S activation (n), and interaction parameters describing the effect on k_{cat} of H2TPPS binding (σ).

	h20S + H2TPPS
K_{AU} (M^{-1})	2.0 (±0.4) ×10^4
K_{BU} (M^{-1})	1.5 (±0.3) ×10^9
K_{AL} (M^{-1})	1.2 (±0.3) ×10^5
K_{BL} (M^{-1})	2.3 (±0.4) ×10^9
n	2
σ_A	1.0 ± 0.2
σ_B	1.8 ± 0.3

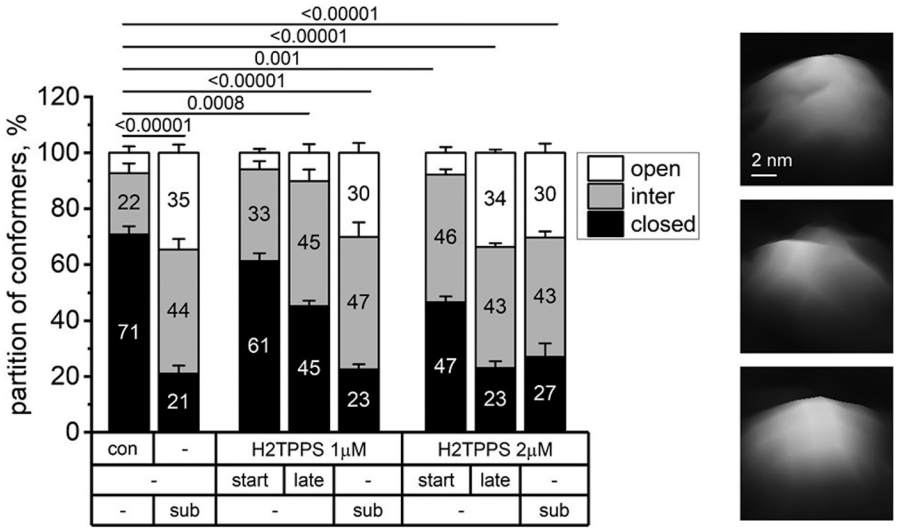

Figure 4. Relative (%) partitions of the three conformational forms of h20S (from the top: open, intermediate and closed; AFM images at the right). Data are reported in the absence (control; "con") and in the presence of 1 µM (central set of columns) or 2 µM (rightmost set of columns) H2TPPS within and over 15 min after its addition ("start" and "late" columns, respectively). The effect of adding the substrate (Suc-LLVY-AMC 100 µM) at both H2TPPS concentrations is also reported ("+Sub" columns). All values are the average of partitions calculated for at least $n = 3$ fields with at least 150 proteasome particles. The partitions between control and substrate or porphyrin treated h20S were statistically different with p values at the top (Chi-Square test). The AFM images are pseudo-3D renderings of zoomed in h20S particles.

Then, we mapped all the positively charged residues of h20S (closed, open, and semi-open conformation) involved in ionic interactions with RPs (i.e. 19S, PA200, PA28; Figure S1; Tables S1–S6) and fitted the resulting map with the pharmacophore of H2TPPS. Results disclosed two clusters of four solvent exposed positively charged amino acids on the α-ring of h20S (edging the α1-α2 and α3-α4 grooves, respectively) which could fit the planar, rigid and negatively charged pharmacophore of H2TPPS (Figure S1; Tables S7–S8). The ligand was positioned in the identified sites and, accordingly, two ligand starting poses were produced. Since H2TPPS was docked to the closed, open, and semi-open conformations of h20S, then a total of six different starting complexes were subjected to docking simulations.

Docking calculations

During the entire docking procedure, the system (i.e. the ligand and the protein) was considered as flexible and the whole h20S structure was defined as search space and included in the calculations. Conformational restraints were applied only to the backbone atoms of conserved secondary structures and scaled during the molecular dynamics (MD) run besides, the generated complexes were subjected to a final round of unconstrained energy minimisation.

Each simulation produced a maximum number of 20 docked complexes (Figures S2–S7). The generated complexes were filtered according to the ligand conformational energy and ranked according to the ligand-protein interaction energy, calculated for each protein residue (Tables S9–S12). Then, for each set of docking calculations, the complex with the most favourable ligand-protein non-bond interaction energy was selected (Table 3).

Protein structural quality of the selected complexes was checked using Molprobity structure evaluator[73] and compared to that of the reference Protein Data Bank (PDB) structure (Table S13).

The ligand explored the whole h20S structure and several putative binding sites were identified as well as ligand-induced protein conformational changes were observed in the generated complexes (Figures S2–S7). In agreement with our binding hypothesis, the complexes with the higher ligand-protein interaction energy showed H2TPPS bound to the α1–α2 and α3–α4 grooves (Table 3). In particular, to the α3–α4 groove when docking H2TPPS to the h20S open conformation and to the α1–α2 groove when docking H2TPPS to the h20S closed conformation. These two complexes showed a similar binding energy, with a ΔE of about 1.5 kcal/mol in favour of the binding to the open conformation. On the other hand, when we used the h20S semi-open conformation as a docking starting sucture, the best docked complexes showed H2TPPS bound at α1–α2 or α3–α4 groove (Figures S8–S9) with an almost equal interaction energy (ΔE ~ 0.5 kcal/mol), which resulted significantly less favourable compared to those calculated for H2TPPS docked to the open (α3–α4) and closed (α1–α2) h20S conformations (ΔE ~ 18 kcal/mol; Table 3).

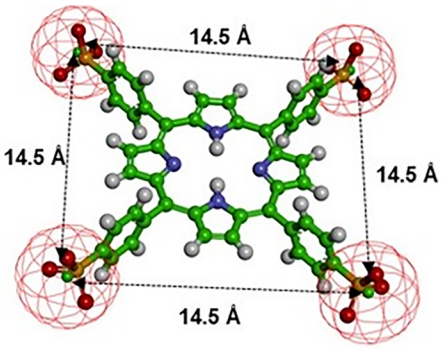

Figure 5. H2TPPS pharmacophore and related inter-atomic distances: (i) the negative ionisable sulphonate groups are evidenced as mesh spheres and (ii) the centroid of the oxygen atoms of each sulphonate group is displayed as a green ball. The global minimum conformer of H2TPPS is displayed in ball & stick and coloured by atom type (C: green; N: blue; S: yellow; O: red and H: white).

Importantly, as can be observed in Figure 6, the binding of H2TPPS at the α1–α2 groove of closed h20S induced the displacement of the N-terminal tail of α2, α3, and α4 from the centre of the channel, thus bringing about a partial opening of the gate. The N-terminal of α2 is subjected to the greatest conformational change moving from α7 (Tyr119) to α3 (Tyr121), while the N-terminal of α3 and α4 lost key interactions[74] with the α6-loop and α5-loop of the α-anulus, respectively (i.e. R3α3-Y123α6 and E126α5-R5α4; Table S14). On the other hand, when h20S is in the open conformation, H2TPPS preferentially binds to the α3-α4 groove forming a stable complex with the gate open.

We then compared the molecular interactions established by H2TPPS with h20S with those established by PA28, PA200, 19S, and a small peptidomimetic ligand (named ZYA) mimicking the activating HbYX-COOH motif[30] (Tables S9–S12). When the anionic porphyrin is bound at the α3–α4 groove (starting h20S conformation: open), it interacts with seven positively charged residues which are also engaged in the binding of h20S to endogenous RPs and ZYA (i.e. R17 (α3), K27 (α4), K28 (α4), K47 (α4), K48 (α4), K52 (α4), and R163 (α4) (Figure 7) (Table S10). Similarly, H2TPPS bound at the α1–α2 groove (starting h20S conformation: closed) interacts with five positively charged residues which are also engaged in the binding of h20S to endogenous RPs and ZYA (R21 (α1), K30(α1), K51 (α2), K53 (α2), and K64 (α2)) (Figure 8; Table S9).

These results support our hypothesis[66] that charged porphyrins exploit a sort of electrostatic code present on the alpha-ring surface, which serves the anchoring of RPs and takes part to the allosteric network leading to gate opening[67,69]. In particular, K30 (α1) and K64 (α2) were reported to be crucial residues for the activation of 20S by the C-terminal tails of 19S and PA200[9,46], while R21 (α1) and R17 (α3) are part of the inverse Pro-loop present at the N-terminal of the α-subunits (P-loop). The interaction of this latter with an invariant PA28 motif between helices 2 and 3, known as the activation loop and containing a conserved glutamate residue, is responsible for gate opening[75]. Similarly, the ligand-induced conformational change of the P-loop of the α2-, α3-, and α4-subunits, is responsible for the displacement of the corresponding N-terminals from the centre of the gate when H2TPPS is docked to the h20S closed conformation (Figures 6 and 8A–B).

Besides charged residues, H2TPPS is also involved in the interaction with other residues engaged in the binding of h20S to endogenous RPs (Figures 7 and 8; Tables S9 and S10), including

Table 3. Interaction energies (kcal/mol) of the best h20S-H2TPPS complexes obtained by docking calculations.

Groove	Starting h20S conformation	Ligand-protein interaction energy (kcal/mol)		
		Tot	vdW	Electrostatic
α1–α2	Closed	−130.57	−80.97	−49.60
α3–α4	Closed	−41.07	−21.58	−19.49
α1–α2	Open	−96.29	−71.77	−24.52
α3–α4	Open	−132.15	−79.17	−52.98
α1–α2	Semi-open	−113.81	−68.98	−44.83
α3–α4	Semi-open	−113.26	−72.69	−40.56

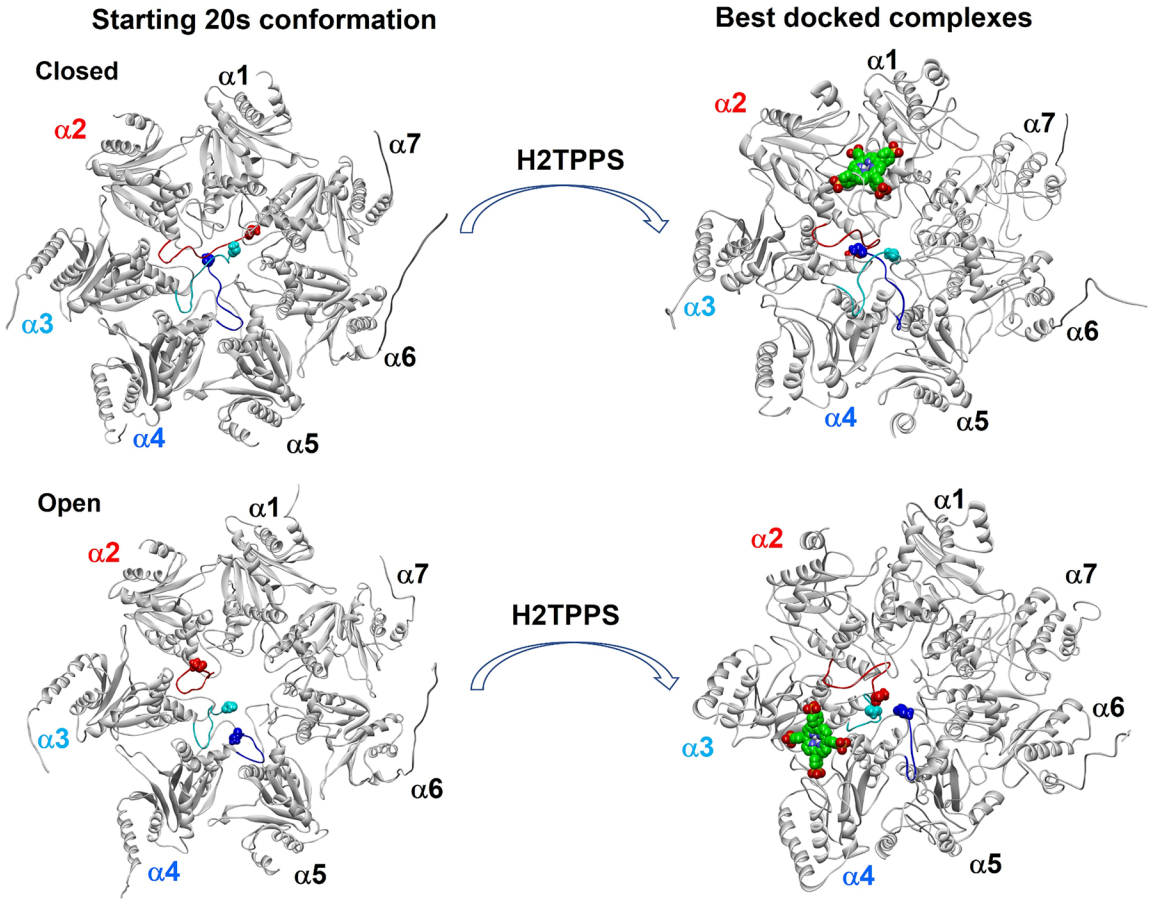

Figure 6. Results of dynamic docking of H2TPPS to h20S: starting protein conformation and final docked complex (top view; only the α-ring is displayed for sake of clarity). The N-terminal tails of the α2, α3, and α4 subunits of h20S are coloured in red, cyan, and blue, respectively, and their first residue displayed as CPK. H2TPPS is displayed as CPK and coloured by atom type, h20S secondary structure is displayed as white ribbon.

the highly conserved hydrophobic residue at the edge of the h20S αH1 helix (M79 (α2); L76 (α4)), which is proved to be a key element in the allosteric network leading to gate opening[76] and to be engaged in the binding with the HbYX activating motif[23,30]. Noteworthy, also the previously studied activating porphyrins (TrisT4 and TMPC) reproduced this crucial interaction, but they were not able to bind the P-loop and, accordingly, did not induce the displacement of the α2-, α3-, and α4-N-terminals from the centre of the gate, as instead was observed when H2TPPS is docked to the h20S closed conformation (Figures 6 and 8A–B).

Discussion

In the presented study we tested a hypothesis of the existence of an electrostatic key code on the 20S proteasome α-surface (Figure 9) matching complementary charged residues on the RP contacting surface (Tables S1–S6). Namely, we postulate that this set of RPs/CP ionic contacts could be exploited to identify or design small-molecule modulators of the h20S catalytic activity[66–69].

On these bases, we expanded our SAR studies on charged porphyrin-based ligands and investigated the activity of the tetra-anionic porphyrin H2TPPS. The results of our multiple methods approach (enzymatic activity, AFM, and dynamic docking studies) clearly demonstrate that H2TPPS is able to modulate the open/closed - gate conformational equilibrium of h20S. Previous structural studies based on cryogenic electron microscopy (cryo-EM) and Nuclear Magnetic Resonance (NMR) techniques showed that such conformational transition is characterised by several intermediate states with some of them corresponding grossly to the semi-open conformation of the gate[23,76,77]. Our AFM data confirmed the presence of semi-open intermediates of the h20S and showed that the treatment with H2TPPS shifts the conformational equilibrium towards the opening of the gate, consequently marked by lowered participation of the closed-gate conformers and elevated partition of the intermediate and open-gate states.

Previous molecular docking studies on porphyrins (i.e. TrisT4 and TMPC)[66,67] or other small-ligand positive allosteric modulators[31,59,78–80] showed the ability of these molecules to interact with different grooves present on the α-surface of 20S proteasome. Our computational studies confirmed these results highlighting a scenario in which H2TPPS could bind to both the closed and open conformers of the h20S with a comparable binding energy (slightly more favourable for the open) but preferring a different α-groove according to the h20S conformational state. By binding to the α1–α2 groove of closed h20S, H2TPPS is able to promote h20S gate opening exploiting the RP interaction sites (induced fit activation mechanism). At the same time, the binding of H2TPPS to the h20S α3–α4 groove could stabilise the open gate conformation (conformational selection activation mechanism). Both phenomena could contribute to the observed shift of the equilibrium towards the opening of the h20S gate in the presence of the ligand and the consequent augmentation of the catalytic activity.

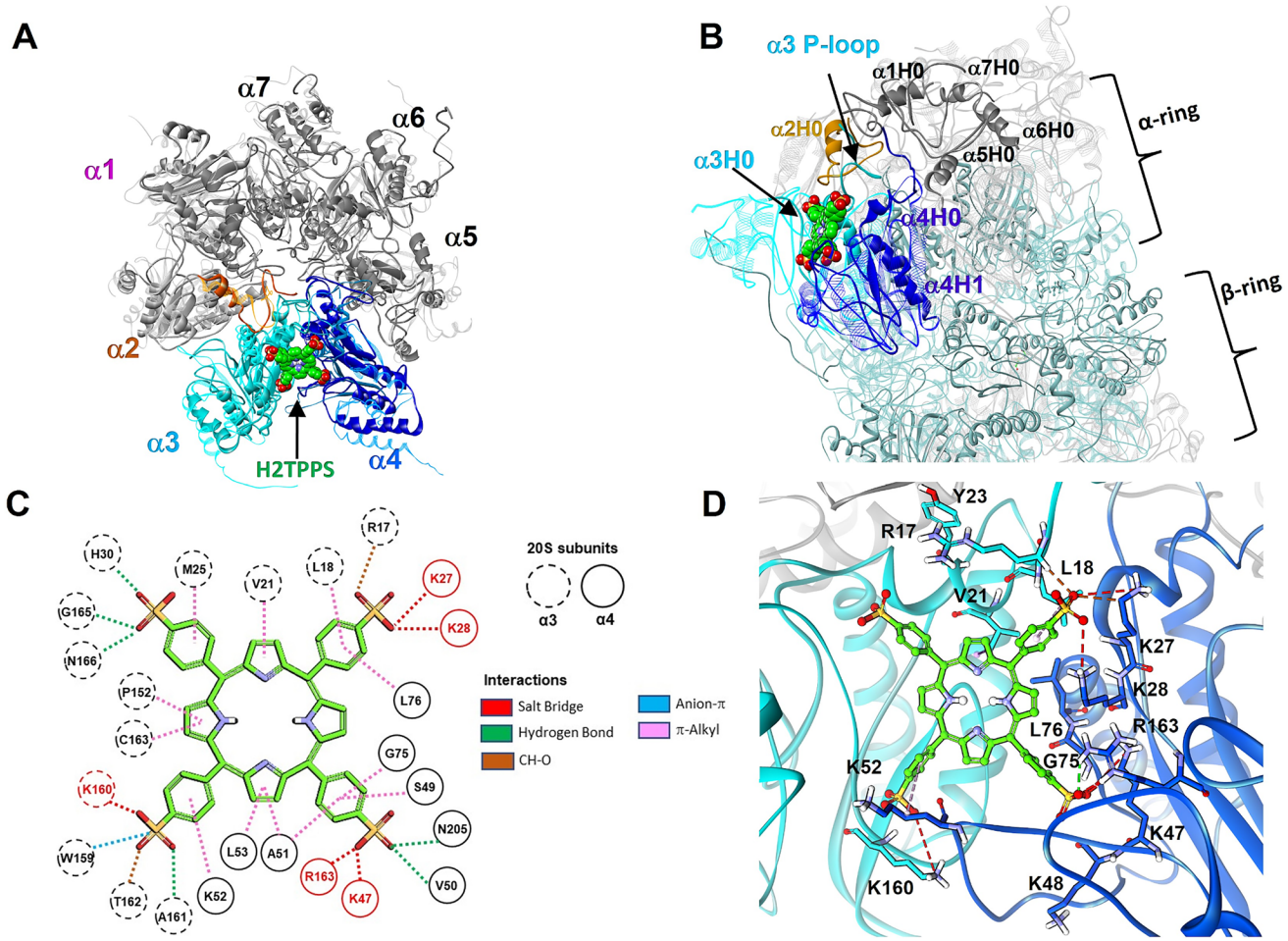

Figure 7. Selected complex of H2TPPS docked to h20S open conformation. (A) Top-view of the α-ring of the resulting complex (solid ribbons) superimposed on the starting h20S structure (line ribbons), H2TPPS is displayed in CPK. (B) Lateral view of the H2TPPS-h20S complex. (C) Schematic representation of the interactions between H2TPPS and h20S residues. (D) close up view of H2TPPS (ball&stick; carbons: green) bound to h20S α3–α4 groove; only protein residues establishing ionic interactions and/or also involved in the binding of h20S to endogenous RPs or ZYA are displayed and labelled. Only polar hydrogens are displayed for clarity.

Thus, computational data are in full agreement with and could provide explanations for experimental observations by AFM and enzymatic activity studies. Indeed, experimental results indicate that treatments with the high concentration (≥ 2 μM) of H2TPPS leads to the lowest achievable participation of closed-gate forms and the highest participation of intermediate and open-gate conformers. Interestingly, such partition is observed also for the substrate-treated proteasomes fully engaged in catalytic activity. These proteasomes experience allosteric signalling "from the inside", that is, from the active chamber to the α face[70]. Binding of H2TPPS to the α face would mimic the effects of allosteric gate opening "from the outside", as it occurs with the RPs. Thanks to the porphyrin binding the core proteasome becomes receptive to the substrates and "activated". According to kinetic studies (Scheme 1), at intermediate H2TPPS concentrations, in the absence of substrate, the predominant populations, almost equally populated, are the E_AX and E_BX states, as indicated by $L_U{\cdot}\gamma$ (i.e. $L_U{\cdot}(K_{BU}/K_{AU}) = 0.22$). Thus, these functional states should correspond to the h20S conformational equilibrium caught by AFM at H2TPPS 1 μM (Figure 4, bar: 1 μM H2TPPS late). Under these conditions, according to Scheme 1, substrate addition induces the formation of the E_AX-S and E_BX-S states, whose conformational equilibrium constant is defined by $L_L{\cdot}\delta$ (i.e. $L_L{\cdot}(K_{BL}/K_{AL}) = 0.74$). This is in line with the concerted action of 1 μM of H2TPPS and substrate in shifting the equilibrium to gate opening observed by AFM (Figure 4, bar: 1 μM H2TPPS + sub). Thus, it is possible to postulate that the conformational equilibria observed by AFM at intermediate H2TPPS concentrations, could correspond to the E_AX, E_BX (without substrate) and E_AX-S, E_BX-S (in the presence of substrate) functional states.

On the other hand, at higher H2TPPS concentrations, the porphyrin binding sites are fully occupied, and the only functional state is, essentially, E_BX_2, which could correspond to the conformational equilibrium caught by AFM at 2 μM of H2TPPS (Figure 4, bar: 2 μM H2TPPS late). At this point, the maximum effect of H2TPPS as gate opener is achieved, and, by consequence, substrate addition did not affect the h20S conformational equilibrium, producing the formation of E_BX_2-S, which is scarcely distinguishable from E_BX_2 in terms of gate opening (Figure 4, bar: 2 μM H2TPPS late vs bar: 2 μM H2TPPS + sub).

Comparing the binding properties of H2TPPS to other porphyrin-based activators (such as Tris-T4), it may be worth remarking that H2TPPS shows a much higher (~ 10-fold) affinity for the substrate-bound h20S with respect to Tris-T4[69]. The structural difference with respect to the previously investigated activating porphyrins is due to the presence of the negative charges, which induces a different interaction mode with the α-ring of h20S. According to docking studies, H2TPPS is able not only to reproduce key interactions of the C-terminal HbYX activating motif of RPs but

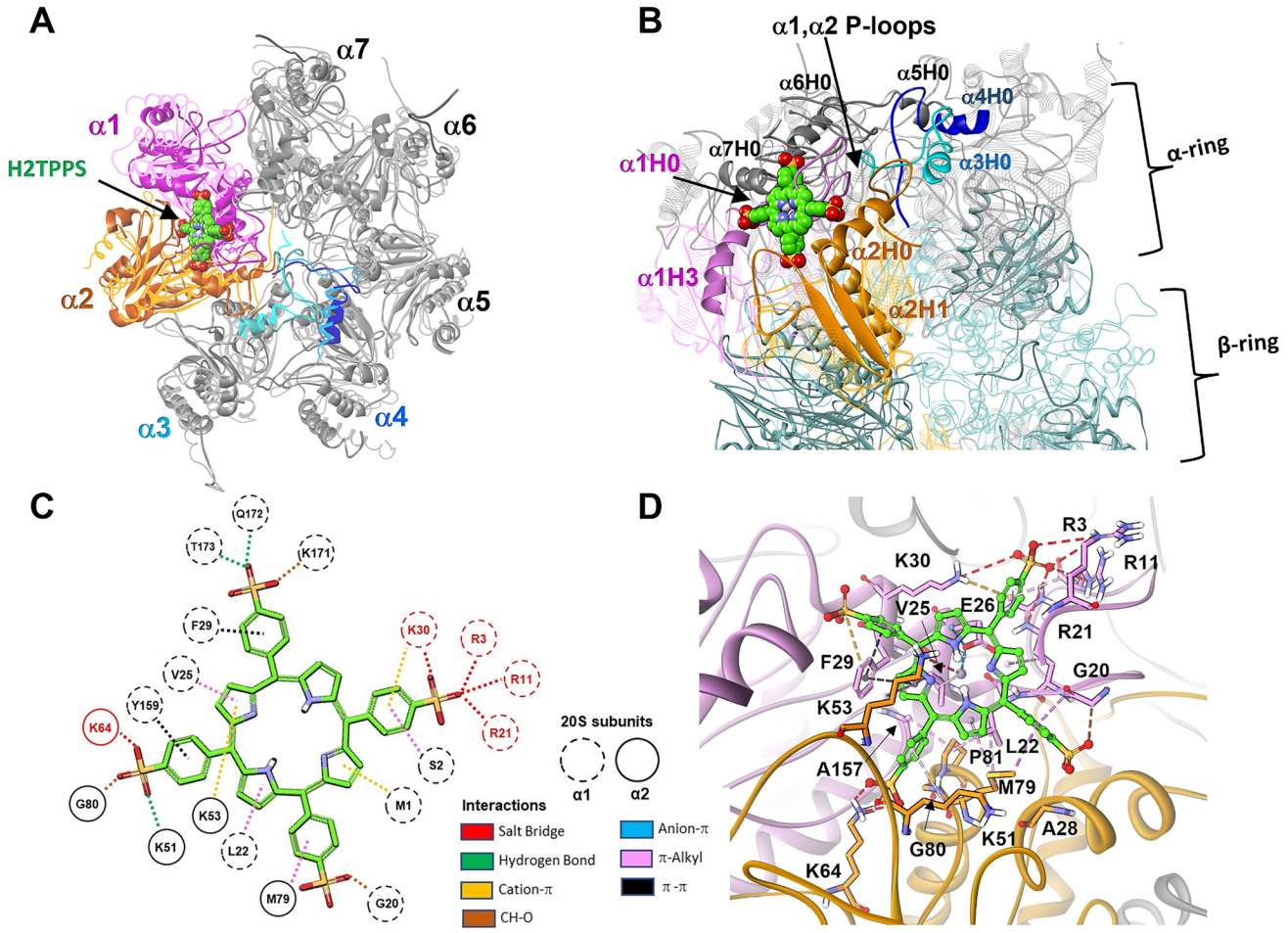

Figure 8. Selected complex of H2TPPS docked to h20S closed conformation. (A) Top-view of the α-ring of the resulting complex (solid ribbons) superimposed on the starting h20S structure (line ribbons), H2TPPS is displayed in CPK. (B) Lateral view of the H2TPPS-h20S complex. (C) Schematic representation of the interactions between H2TPPS and h20S residues. (D) close up view of H2TPPS (ball&stick; carbons: green) bound to h20S α1-α2 groove; only protein residues establishing ionic interactions and/or also involved in the binding of h20S to endogenous RPs or ZYA are displayed and labelled. Only polar hydrogens are displayed for clarity.

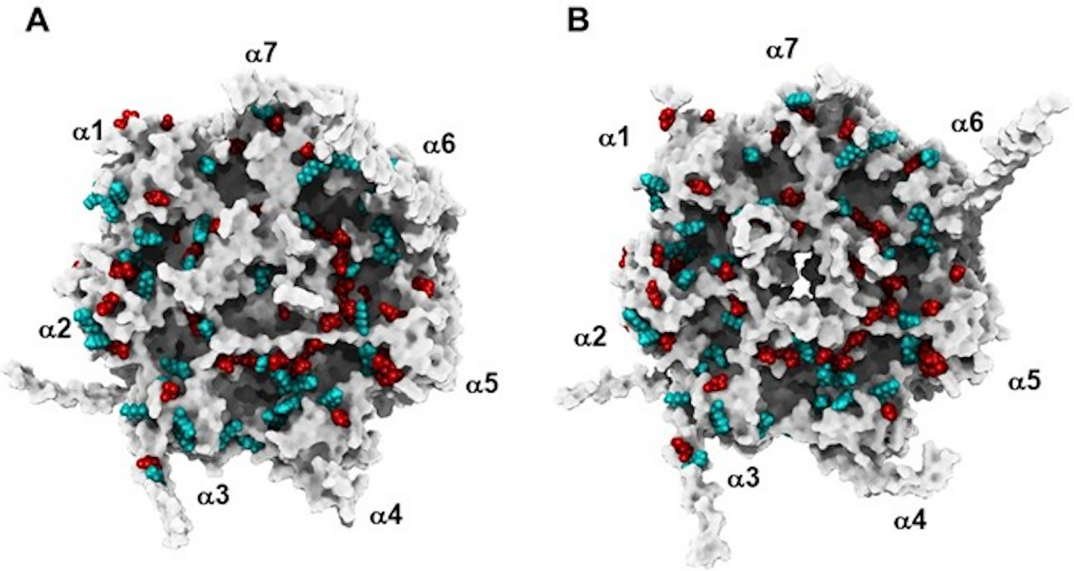

Figure 9. Top view of the experimentally determined structures of h20S proteasome in the closed (A; PDB ID: 4R3O) and open (B; PDB IDs: 6MSK) states. The solvent accessible surface of the protein is displayed in gray. The charged residues involved in ionic interactions with RPs (i.e. 19S, PA28α, and PA200) are mapped and displayed as CPK (positive = cyan; negative = red).

also, when docked to the α1-α2 groove of closed h20S, to interact with the P-loop and to induce the displacement of the α2, α3, and α4 N-terminal tails from the centre of the gate, thus mimicking the activation loop of PA28. This could explain why two molecules of H2TPPS are sufficient to induce the observed rate enhancement, whilst in the case of Tris-T4 three molecules are required for the full activation effect[69]. Moreover, since only two H2TPPS molecules accommodate in the grooves, a less crowded occupancy of the α-ring compared to TrisT4 can be foreseen, and this could be related to the absence of any inhibitory effect even at high substrate concentrations (as it occurred in the case of Tris-T4).

Conclusions

A complementary set of experimental and computational studies has collectively confirmed that H2TPPS, at a low micromolar level, is an allosteric modulator of h20S proteasome capable of activating ChT-L activity. Molecular models match experimental data indicating that H2TPPS binding to h20S proteasome induces the shifting of the conformational equilibrium towards the open conformation of the substrate gate. As predicted by the fit of the tetra-anionic H2TPPS pharmacophore with h20S positively charged residues involved in electrostatic interactions with RPs, H2TPPS is able to reproduce the key structural elements of RPs responsible for binding to h20S charged hot spots. Importantly, unlike other RP-derived proteasome activators (including the previously investigated porphyrins), H2TPPS not only reproduces key interactions of the C-terminal HbYX activating motif of 19S and PA200 but also those of the activation loop of PA28, an invariant motif containing conserved negatively charged glutamate residues. As a result, H2TPPS exhibits greater efficiency also compared to other charged porphyrins, such as TrisT4. The results herein presented support the rational discovery of small ligands mimicking the key structural elements of 20S RPs as a viable approach to search for new chemical scaffolds acting as proteasome activators. In the light of its functional and structural properties, H2TPPS could be employed as a novel type of "lead compound" to guide drug-discovery approaches aimed at activating proteasomal degradation to treat neurodegenerative diseases.

Author contributions

Conceptualisation, M.C., A.M.S., C.F.; Data curation, A.C., A.D., M.P., O.T., D.S.; Formal analysis, D.M., M.P., M.C., M.G., P.O., A.M.S., C.F.; Funding acquisition D.M., A.M.S., C.F., G.T.; Investigation M.P., A.C., A.D., O.T., D.S., A.M.S., C.F.; Methodology M.G., P.O., M.C., A.M.S., C.F., R.P., M.P.; Project administration M.C., A.M.S., C.F.; Resources R.P.; Software M.P., O.T., C.F.; Supervision A.M.S., C.F., M.C., M.G., P.O., D.M.; Visualisation C.F., M.P., O.T., G.T., A.C.; Writing – original draft M.C., A.M.S., C.F. All authors reviewed and edited the manuscript and approved the final version.

Disclosure statement

The authors declare no conflict of interest.

Funding

This study was financially supported by the Italian Ministry of University and Research (MUR): "PRIN 2022 PNRR Prot. P2022YRPHS-Financed by European Union - Next Generation EU, Mission 4 Component C2, CUP: E53D23016180001; B53D23025960001"; "PRIN Prot. 2022PAAYZE -Financed by European Union - Next Generation EU, Mission 4 Component 1, CUP: E53D23010000006; B53D23016440006"; "PRIN Prot.2022R9WCZS -Financed by European Union - Next Generation EU, Mission 4 Component 1, CUP: E53D23010020001; E53D23010030006"; 2023 William & Ella Owens Medical Research Foundation (MG and PAO). The support of "Fondazione Roma" and Ministry of Health is gratefully acknowledged. Also supported by Ministero dell'Istruzione, dell'Università e della Ricerca.

Data availability statement

The data that support the findings of this study are available from the corresponding authors, [M.C. and C.F.], upon reasonable request.

References

1. Ciechanover A. Proteolysis: from the lysosome to ubiquitin and the proteasome. Nat Rev Mol Cell Biol. 2005;6(1):79–87.
2. Glickman MH, Ciechanover A. The ubiquitin-proteasome proteolytic pathway: destruction for the sake of construction. Physiol Rev. 2002;82(2):373–428.
3. Livneh I, Cohen-Kaplan V, Cohen-Rosenzweig C, Avni N, Ciechanover A. The life cycle of the 26S proteasome: from birth, through regulation and function, and onto its death. Cell Res. 2016;26(8):869–885.
4. Tomko RJ, Hochstrasser M. Molecular architecture and assembly of the eukaryotic proteasome. Annu Rev Biochem. 2013;82(1):415–445.
5. Klaips CL, Jayaraj GG, Hartl FU. Pathways of cellular proteostasis in aging and disease. J Cell Biol. 2018;217(1):51–63.
6. Thibaudeau TA, Smith DM. A practical review of proteasome pharmacology. Pharmacol Rev. 2019;71(2):170–197.
7. Tundo GR, Sbardella D, Santoro AM, Coletta A, Oddone F, Grasso G, Milardi D, Lacal PM, Marini S, Purrello R, et al. The proteasome as a druggable target with multiple therapeutic potentialities: cutting and non-cutting edges. Pharmacol Ther. 2020;213:107579.
8. Schweitzer A, Aufderheide A, Rudack T, Beck F, Pfeifer G, Plitzko JM, Sakata E, Schulten K, Förster F, Baumeister W. Structure of the human 26S proteasome at a resolution of 3.9 Å. Proc Natl Acad Sci U S A. 2016;113(28):7816–7821.
9. Toste Rêgo A, da Fonseca PCA. Characterization of fully recombinant human 20s and 20s-PA200 proteasome complexes. Mol Cell. 2019;76(1):138–147.e5.
10. Zhao J, Makhija S, Zhou C, Zhang H, Wang Y, Muralidharan M, Huang B, Cheng Y. Structural insights into the human PA28–20S proteasome enabled by efficient tagging and purification of endogenous proteins. Proc Natl Acad Sci U S A. 2022;119(33):e220720011.
11. Choi WH, Yun Y, Byun I, Kim S, Lee S, Sim J, Levi S, Park SH, Jun J, Kleifeld O, et al. ECPAS/ECM29-mediated 26S proteasome disassembly is an adaptive response to glucose starvation. Cell Rep. 2023;42(7):112701.
12. Kalderon B, Kogan G, Bubis E, Pines O. Cytosolic HSP60 can modulate proteasome activity in yeast. J Biol Chem. 2015;290(6):3542–3551.
13. Sbardella D, Tundo GR, Coletta A, Marcoux J, Koufogeorgou EI, Ciaccio C, Santoro AM, Milardi D, Grasso G, Cozza P, et al. The insulin-degrading enzyme is an allosteric modulator of

the 20S proteasome and a potential competitor of the 19s. Cell Mol Life Sci. 2018;75(18):3441–3456.
14. Deshmukh FK, Ben-Nissan G, Olshina MA, Füzesi-Levi MG, Polkinghorn C, Arkind G, Leushkin Y, Fainer I, Fleishman SJ, Tawfik D, et al. Allosteric regulation of the 20S proteasome by the catalytic core regulators (CCRS) family. Nat Commun. 2023;14(1):3126.
15. Gaczynska M, Osmulski PA. Targeting protein–protein interactions in the ubiquitin–proteasome pathway. Adv Protein Chem Struct Biol. 2018;110:123–165.
16. Guerrero C, Milenkovic T, Przulj N, Kaiser P, Huang L. Characterization of the proteasome interaction network using a QTAX-based tag-team strategy and protein interaction network analysis. Proc Natl Acad Sci U S A. 2008;105(36):13333–13338.
17. Groll M, Ditzel L, Löwe J, Stock D, Bochtler M, Bartunik HD, Huber R. Structure of 20S proteasome from yeast at 2.4Å resolution. Nature. 1997;386(6624):463–471.
18. Harshbarger W, Miller C, Diedrich C, Sacchettini J. Crystal structure of the human 20S proteasome in complex with carfilzomib. Structure. 2015;23(2):418–424.
19. Groll M, Heinemeyer W, Jäger S, Ullrich T, Bochtler M, Wolf DH, Huber R. The catalytic sites of 20s proteasomes and their role in subunit maturation: a mutational and crystallographic study. Proc Natl Acad Sci U S A. 1999;96(20):10976–10983.
20. Chen S, Wu J, Lu Y, Ma Y-B, Lee B-H, Yu Z, Ouyang Q, Finley DJ, Kirschner MW, Mao Y. Structural basis for dynamic regulation of the human 26S proteasome. Proc Natl Acad Sci U S A. 2016;113(46):12991–12996.
21. Chuah JJ, Rexroad MS, Smith DM. High resolution structures define divergent and convergent mechanisms of archaeal proteasome activation. Commun Biol. 2023;6(1):733.
22. Collins GA, Goldberg AL. The logic of the 26S proteasome. Cell. 2017;169(5):792–806.
23. Dong Y, Zhang S, Wu Z, Li X, Wang WL, Zhu Y, Stoilova-McPhie S, Lu Y, Finley D, Mao Y. Cryo-EM structures and dynamics of substrate-engaged human 26S proteasome. Nature. 2019;565(7737):49–55.
24. Whitby FG, Masters EI, Kramer L, Knowlton JR, Yao Y, Wang CC, Hill CP. Structural basis for the activation of 20s proteasomes by 11S regulators. Nature. 2000;408(6808):115–120.
25. Zhang Z, Clawson A, Realini C, Jensen CC, Knowlton JR, Hill CP, Rechsteiner M. Identification of an activation region in the proteasome activator rega. Proc Natl Acad Sci U S A. 1998;95(6):2807–2811.
26. Cromm PM, Crews CM. The proteasome in modern drug discovery: second life of a highly valuable drug target. ACS Cent Sci. 2017;3(8):830–838.
27. Fernández-Cruz I, Reynaud E. Proteasome subunits involved in neurodegenerative diseases. Arch Med Res. 2021;52(1):1–14.
28. Thibaudeau TA, Anderson RT, Smith DM. A common mechanism of proteasome impairment by neurodegenerative disease-associated oligomers. Nat Commun. 2018;9(1):1097.
29. Kageyama M, Ota T, Sasaoka M, Katsuta O, Shinomiya K. Chemical proteasome inhibition as a novel animal model of inner retinal degeneration in rats. PLoS One. 2019;14(5):e0217945.
30. Chuah JJ, Thibaudeau TA, Smith DM. Minimal mechanistic component of HbYX-dependent proteasome activation that reverses impairment by neurodegenerative-associated oligomers. Commun Biol. 2023;6(1):725.
31. Fiolek TJ, Keel KL, Tepe JJ. Fluspirilene analogs activate the 20S proteasome and overcome proteasome impairment by intrinsically disordered protein oligomers. ACS Chem Neurosci. 2021;12(8):1438–1448.
32. Njomen E, Tepe JJ. Proteasome activation as a new therapeutic approach to target proteotoxic disorders. J Med Chem. 2019;62(14):6469–6481.
33. Wang X, Wang H. Priming the proteasome to protect against proteotoxicity. Trends Mol Med. 2020;26(7):639–648.
34. Chocron ES, Munkácsy E, Kim HS, Karpowicz P, Jiang N, Van Skike CE, DeRosa N, Banh AQ, Palavicini JP, Wityk P, et al. Genetic and pharmacologic proteasome augmentation ameliorates Alzheimer's-like pathology in mouse and fly app overexpression models. Sci Adv. 2022;8(23):eabk2252.
35. Du Z, Chakrabarti S, Kulaberoglu Y, Smith ES, Dobson CM, Itzhaki LS, Kumita JR. Probing the unfolded protein response in long-lived naked mole-rats. Biochem Biophys Res Commun. 2020;529(4):1151–1157.
36. Rodriguez KA, Edrey YH, Osmulski P, Gaczynska M, Buffenstein R. Altered composition of liver proteasome assemblies contributes to enhanced proteasome activity in the exceptionally long-lived naked mole-rat. PLoS One. 2012;7(5):e35890.
37. Chondrogianni N, Petropoulos I, Franceschi C, Friguet B, Gonos ES. Fibroblast cultures from healthy centenarians have an active proteasome. Exp Gerontol. 2000;35(6-7):721–728.
38. Hipp MS, Kasturi P, Hartl FU. The proteostasis network and its decline in ageing. Nat Rev Mol Cell Biol. 2019;20(7):421–435.
39. Dagar G, Kumar R, Yadav KK, Singh M, Pandita TK. Ubiquitination and deubiquitination: implications on cancer therapy. Biochim Biophys Acta Gene Regul Mech. 2023;1866(4):194979.
40. Mathien S, Tesnière C, Meloche S. Regulation of mitogen-activated protein kinase signaling pathways by the Ubiquitin-proteasome system and its pharmacological potential. Pharmacol Rev. 2021;73(4):263–296.
41. Zheng L-L, Wang L-T, Pang Y-W, Sun L-P, Shi L. Recent advances in the development of deubiquitinases inhibitors as antitumor agents. Eur J Med Chem. 2024;266:116161.
42. Cekała K, Trepczyk K, Sowik D, Karpowicz P, Giełdoń A, Witkowska J, Giżyńska M, Jankowska E, Wieczerzak E. Peptidomimetics based on C-terminus of BLM10 stimulate human 20S proteasome activity and promote degradation of proteins. Biomolecules. 2022;12(6):777.
43. Gillette TG, Kumar B, Thompson D, Slaughter CA, DeMartino GN. Differential roles of the COOH termini of AAA subunits of PA700 (19 s regulator) in asymmetric assembly and activation of the 26 S proteasome. J Biol Chem. 2008;283(46):31813–31822.
44. Jones CL, Tepe JJ. Proteasome activation to combat proteotoxicity. Molecules. 2019;24(15):2841.
45. Opoku-Nsiah KA, de la Pena AH, Williams SK, Chopra N, Sali A, Lander GC, Gestwicki JE. The YΦ motif defines the structure-activity relationships of human 20S proteasome activators. Nat Commun. 2022;13(1):1226.
46. Smith DM, Chang S-C, Park S, Finley D, Cheng Y, Goldberg AL. Docking of the proteasomal ATPases' carboxyl termini in the 20S proteasome's α ring opens the gate for substrate entry. Mol Cell. 2007;27(5):731–744.
47. Giżyńska M, Witkowska J, Karpowicz P, Rostankowski R, Chocron ES, Pickering AM, Osmulski P, Gaczynska M, Jankowska E. Proline- and arginine-rich peptides as flexible allosteric modulators of human proteasome activity. J Med Chem. 2019;62(1):359–370.
48. Osmulski PA, Karpowicz P, Jankowska E, Bohmann J, Pickering AM, Gaczyńska M. New peptide-based pharmacophore activates 20S proteasome. Molecules. 2020;25(6):1439.
49. Farzan M, Farzan M, Shahrani M, Navabi SP, Vardanjani HR, Amini-Khoei H, Shabani S. Neuroprotective properties of

Betulin, betulinic acid, and ursolic acid as triterpenoids derivatives: a comprehensive review of mechanistic studies. Nutr Neurosci. 2024;27(3):223–240.
50. Dang Z, Jung K, Qian K, Lee K-H, Huang L, Chen C-H. Synthesis of lithocholic acid derivatives as proteasome regulators. ACS Med Chem Lett. 2012;3(11):925–930.
51. Yilmaz S, Bedir E, Ballar Kirmizibayrak P. The role of cycloastragenol at the intersection of Nrf2/are, telomerase, and proteasome activity. Free Radic Biol Med. 2022;188:105–116.
52. Carmona V, Martín-Aragón S, Goldberg J, Schubert D, Bermejo-Bescós P. Several targets involved in alzheimer's disease amyloidogenesis are affected by Morin and Isoquercitrin. Nutr Neurosci. 2020;23(8):575–590.
53. Khan TK, You Y, Nelson TJ, Kundu S, Pramanik SK, Das J. Modulation of proteasome activity by curcumin and didemethylcurcumin. J Biomol Struct Dyn. 2022;40(18):8332–8339.
54. Amici M, Cecarini V, Pettinari A, Bonfili L, Angeletti M, Barocci S, Biagetti M, Fioretti E, Maria Eleuteri A. Binding of aflatoxins to the 20S proteasome: effects on enzyme functionality and implications for oxidative stress and apoptosis. Biol Chem. 2007;388(1):107–117.
55. Persico M, García-Viñuales S, Santoro AM, Lanza V, Tundo GR, Sbardella D, Coletta M, Romanucci V, Zarrelli A, Di Fabio G, et al. Silybins are stereospecific regulators of the 20S proteasome. Bioorg Med Chem. 2022;66:116813.
56. Chondrogianni N, Chinou I, Gonos ES. Anti-aging properties of the olive constituent oleuropein in human cells. In: Olives and olive oil in health and disease prevention. Cambridge, MA: Academic Press; 2010. p. 1335–1343.
57. Sbardella D, Coletta A, Tundo GR, Ahmed IMM, Bellia F, Oddone F, Manni G, Coletta M. Structural and functional evidence for citicoline binding and modulation of 20S proteasome activity: novel insights into its pro-proteostatic effect. Biochem Pharmacol. 2020;177:113977.
58. Sadahiro Y, Nishimura S, Hitora Y, Tsukamoto S. Syrosingopine enhances 20S proteasome activity and degradation of α-synuclein. J Nat Prod. 2024;87(3):554–559.
59. George DE, Tepe JJ. Advances in proteasome enhancement by small molecules. Biomolecules. 2021;11(12):1789.
60. Santoro AM, Lanza V, Bellia F, Sbardella D, Tundo GR, Cannizzo A, Grasso G, Arizzi M, Nicoletti VG, Alcaro S, et al. Pyrazolones activate the proteasome by gating mechanisms and protect neuronal cells from β-amyloid toxicity. ChemMedChem. 2020;15(3):302–316.
61. Njomen E, Osmulski PA, Jones CL, Gaczynska M, Tepe JJ. Small molecule modulation of Proteasome Assembly. Biochemistry. 2018;57(28):4214–4224.
62. Liao EE, Yang M, Nathan Kochen N, Vunnam N, Braun AR, Ferguson DM, Sachs JN. Proteasomal stimulation by MK886 and its derivatives can rescue tau-induced neurite pathology. Mol Neurobiol. 2023;60(10):6133–6144.
63. Halder S, Macatangay NJ, Zerfas BL, Salazar-Chaparro AF, Trader DJ. Oleic amide derivatives as small molecule stimulators of the human proteasome's core particle. RSC Med Chem. 2022;13(9):1077–1081.
64. Ban HS, Minegishi H, Shimizu K, Maruyama M, Yasui Y, Nakamura H. Discovery of carboranes as inducers of 20S Proteasome activity. ChemMedChem. 2010;5(8):1236–1241.
65. Coleman RA, Trader DJ. Development and application of a sensitive peptide reporter to discover 20S proteasome stimulators. ACS Comb Sci. 2018;20(5):269–276.
66. Di Dato A, Cunsolo A, Persico M, Santoro AM, D'Urso A, Milardi D, Purrello R, Stefanelli M, Paolesse R, Tundo GR, et al. Electrostatic map of proteasome α-rings encodes the design of allosteric porphyrin-based inhibitors able to affect 20s conformation by cooperative binding. Sci Rep. 2017;7(1):17098.
67. Persico M, Santoro AM, D'Urso A, Milardi D, Purrello R, Cunsolo A, Gobbo M, Fattorusso R, Diana D, Stefanelli M, et al. Modulation of the 20S proteasome activity by porphyrin derivatives is steered through their charge distribution. Biomolecules. 2022;12(6):741.
68. Santoro AM, Cunsolo A, D'Urso A, Sbardella D, Tundo GR, Ciaccio C, Coletta M, Diana D, Fattorusso R, Persico M, et al. Cationic porphyrins are tunable gatekeepers of the 20S proteasome. Chem Sci. 2016;7(2):1286–1297.
69. Santoro AM, D'Urso A, Cunsolo A, Milardi D, Purrello R, Sbardella D, Tundo GR, Diana D, Fattorusso R, Dato AD, et al. Cooperative binding of the cationic porphyrin tris-T4 enhances catalytic activity of 20S proteasome unveiling a complex distribution of functional states. Int J Mol Sci. 2020;21(19):7190.
70. Osmulski PA, Hochstrasser M, Gaczynska M. A tetrahedral transition state at the active sites of the 20S proteasome is coupled to opening of the α-ring channel. Structure. 2009;17(8):1137–1147.
71. Giletto MB, Osmulski PA, Jones CL, Gaczynska ME, Tepe JJ. Pipecolic esters as minimized templates for proteasome inhibition. Org Biomol Chem. 2019;17(10):2734–2746.
72. Güleç Ö, Türkeş C, Arslan M, Işık M, Demir Y, Duran HE, Fırat M, Küfrevioğlu Öİ, Beydemir Ş. Dynamics of small molecule-enzyme interactions: novel benzenesulfonamides as multi-target agents endowed with inhibitory effects against some metabolic enzymes. Arch Biochem Biophys. 2024;759:110099.
73. Davis IW, Leaver-Fay A, Chen VB, Block JN, Kapral GJ, Wang X, Murray LW, Arendall WB, Snoeyink J, Richardson JS, et al. Molprobity: all-atom contacts and structure validation for proteins and nucleic acids. Nucleic Acids Res. 2007;35(Web Server issue):W375–W383.
74. Rabl J, Smith DM, Yu Y, Chang S-C, Goldberg AL, Cheng Y. Mechanism of gate opening in the 20S proteasome by the proteasomal ATPases. Mol Cell. 2008;30(3):360–368.
75. Lesne J, Locard-Paulet M, Parra J, Zivković D, Menneteau T, Bousquet M-P, Burlet-Schiltz O, Marcoux J. Conformational maps of human 20s proteasomes reveal pa28- and immuno-dependent inter-ring crosstalks. Nat Commun. 2020;11(1):6140.
76. Ruschak AM, Kay LE. Proteasome allostery as a population shift between interchanging conformers. Proc Natl Acad Sci USA. 2012;109(50):E3454–E3462.
77. Huang R, Pérez F, Kay LE. Probing the cooperativity of thermoplasma acidophilum proteasome core particle gating by NMR spectroscopy. Proc Natl Acad Sci USA. 2017;114(46):E9846–E9854.
78. Jones CL, Njomen E, Sjögren B, Dexheimer TS, Tepe JJ. Small molecule enhancement of 20S proteasome activity targets intrinsically disordered proteins. ACS Chem Biol. 2017;12(9):2240–2247.
79. Staerz SD, Jones CL, Tepe JJ. Design, synthesis, and biological evaluation of potent 20S proteasome activators for the potential treatment of α-synucleinopathies. J Med Chem. 2022;65(9):6631–6642.
80. Staerz SD, Anamoah C, Tepe JJ. 20S proteasome enhancers prevent cytotoxic tubulin polymerization-promoting protein induced α-synuclein aggregation. iScience. 2024;27(7):110166.